Robotics and Computer-Integrated Manufacturing 29 (2013) 121–128

Contents lists available at SciVerse ScienceDirect

Robotics and Computer-Integrated Manufacturing

journal homepage: www.elsevier.com/locate/rcim

Reconfigurability and unified kinematics modeling of a 3rTPS metamorphic parallel mechanism with perpendicular constraint screws

Dongming Gan [a,*], Jian S. Dai [b], Jorge Dias [a,c], Lakmal Seneviratne [a,b]

[a] Robotics Research Institute, Khalifa University of Science, Technology & Research, 127788 Abu Dhabi, UAE
[b] School of Natural and Mathematical Sciences, King's College London, University of London, London WC2R2LS, UK
[c] Institute of Systems and Robotics, Faculty of Science and Technology, University of Coimbra, Portugal

ARTICLE INFO

Article history:
Received 10 November 2011
Received in revised form
20 November 2012
Accepted 20 November 2012
Available online 3 January 2013

Keywords:
Constraint screw
Reconfiguration
Mobility change
Unified kinematics
Parallel mechanism

ABSTRACT

This paper investigates reconfigurability and unified analytical kinematics analysis of a new 3rTPS metamorphic parallel mechanism consisting of three reconfigurable rTPS limbs in perpendicular base planes. Constraint screw systems show that in one phase the rTPS limb has no constraint to the platform and in the other phase obtained by altering the reconfigurable Hooke joint, it provides a constraint force. The two phases of the limb qualify the 3rTPS metamorphic parallel mechanism to have four topologies with ability of mobility change among 3R (three rotations), 3R1T (three rotations one translation), 3R2T and mobility 6. By considering the difference of the two phases of the limb, a unified kinematics modeling is proposed based on the actuation scheme analysis by taking one phase as a special case of the other. Following this, a unified kinematics modeling of the 3rTPS metamorphic parallel mechanism is obtained by covering all its four topologies. Both inverse and forward kinematics analysis are solved analytically and numerical examples confirm these theoretical results.

1. Introduction

Since Gough [1] used a parallel mechanism for the tire test and Stewart [2] further described it for the flight simulator, parallel mechanism demonstrated great advantages in industry assembly [3,4], manufacturing [5], force transducer [6], rehabilitation [7] and robotics surgery [8] due to its high load-carrying capacity, good positioning accuracy and low inertia [9] with respect to the serial counterparts. Motivated by the applications, various researches have been taken to investigate the basic theories of parallel mechanisms to solve the kinematics [10,11], dynamics [12], workspace [13], optimization [14] and synthesis [15,16] of novel structures. With the requirements of rapid customization and diverse environment changing [17], parallel mechanisms that have reconfigurablility to adapt to different scenarios have attracted much attention in recent mechanism research. Based on this, metamorphic parallel mechanisms (MPMs) [18], which are a class of mechanisms that possess adaptability and reconfigurability to change permanent finite mobility based on topological structure change, were introduced. Metamorphic parallel mechanisms keep the advantages of traditional parallel mechanisms but with ability of reconfiguring and mobility change.

Research of mechanisms that have reconfigurability started in 1990s when Wohlhart [19] presented kinematotropic linkages with variable position parameters and Dai and Rees Jones [20] proposed metamorphic mechanisms in the study of decorative carton folds and reconfigurable packaging. Following this, many contributions have been made on this topic. Parise et al. [21] presented new ortho-planar metamorphic mechanisms. Liu and Yang [22] investigated three metamorphic ways of changing the topological structures of a mechanism. Dai and Rees [23] presented the topology of various mobility configurations of metamorphic mechanisms by using matrix operations while Yan and Kuo [24,25] investigated variable topologies of kinematic joints and presented the topological representation of joints. Based on single-loop and multi-loop kinematotropic chains, Fanghella and Galletti [26] developed kinematotropic parallel mechanisms with variable motions. Refaat and Herve et al. [27] proposed a parallel mechanism with changed motion for machine tool applications. A family of parallel mechanisms that have multiple operation modes with pure translation and pure rotation were presented by Kong et al. [28]. Later, Dai and Wang [29] presented a metamorphic multifingered hand with an articulated palm while Zhang and Dai [30] developed a methodology for synthesis and configuration design of metamorphic mechanisms based on biological modeling and genetic evolution. Recently, Zhang et al. [31] proposed a metamorphic parallel mechanism with the ability of performing phase change and orientation switch by introducing a metamorphic kinematic pair.

* Corresponding author. Tel.: +971 2 5018558; fax: +971 2 4472442.
E-mail addresses: dongming.gan@kustar.ac.ae, gandong64@gmail.com (D. Gan).

0736-5845/$ - see front matter © 2012 Elsevier Ltd. All rights reserved.
http://dx.doi.org/10.1016/j.rcim.2012.11.006

The new metamorphic parallel mechanism proposed in this paper is based on a reconfigurable rT*PS* limb with two topology phases stemming from a reconfigurable Hooke (rT) joint [32]. Based on this rT joint, various metamorphic parallel mechanisms [1,33] have been presented with a general construction method introduced using screw theory [34]. As screws [35] naturally present the relations of geometric constraints among the joints and limbs in parallel mechanisms, they show great advantage in describing the topology change of metamorphic parallel mechanisms as illustrated in this paper.

Since many novel metamorphic parallel mechanisms have been proposed, further analysis, such as kinematics, dynamics and optimization, has not been identified on them. Especially, when considering property changes and variable topologies of a metamorphic parallel mechanism, unified kinematics, dynamics and other interpreting methods are required. A unified kinematics modeling is for the first time investigated in this paper following the topology change of the 3rT*PS* metamorphic parallel mechanism.

In the following, the paper is arranged as: Section 2 introduces the two phases of the rT*PS* limb with its geometric constraint analysis in screw theory; following this, mobility change of the 3rT*PS* metamorphic parallel mechanism is demonstrated in different topologies in Section 3 and possible actuation schemes are discussed in Section 4; based on these, a unified kinematics modeling of the 3rT*PS* metamorphic parallel mechanism is proposed by covering all its topologies in Section 5 with numerical examples illustrating the validity; conclusions make up Section 6.

2. Two phases of the reconfigurable rT*PS* limb

As in Fig. 1, the reconfigurable rT*PS* limb consists of a reconfigurable Hooke (rT) joint, a prismatic joint and a spherical joint. The reconfigurability of this limb stems from the configuration change of the rT joint which has two rotational degrees of freedom (DOFs) about two perpendicularly intersecting rotational axes (radial axis and bracket axis) as in Fig. 1. A grooved ring is used to house the radial axis and make it have the ability of altering its direction by rotating and fixing freely along the groove. This allows the radial rotation axis change with respect to the limb, resulting in two typical phases of the rT*PS* limb as in Fig. 1. In Fig. 1(a), the radial axis is perpendicular to the limb (prismatic joint) which is denoted as phase $(rT)_1PS$. The radial axis is collinear with the limb (prismatic joint) passing through the spherical joint center as in Fig. 1(b) and the limb phase is expressed as $(rT)_2PS$.

Set a limb coordinate system ${}^1o{}^1x{}^1y{}^1z$ at the rT joint center with ${}^1x$ axis collinear with the bracket axis and ${}^1y$ axis perpendicular to the bracket surface as in Fig. 1(a), the twist system of the $(rT)_1PS$ limb is given as

$$\left\{{}^1\mathbf{S}_1\right\}=\left\{\begin{array}{l}{}^1\mathbf{S}_{11}=\begin{bmatrix}1&0&0&0&0&0\end{bmatrix}\\ {}^1\mathbf{S}_{12}=\begin{bmatrix}0&-s\alpha&c\alpha&0&0&0\end{bmatrix}\\ {}^1\mathbf{S}_{13}=\begin{bmatrix}0&0&0&-s\beta&c\beta c\alpha&c\beta s\alpha\end{bmatrix}\\ {}^1\mathbf{S}_{14}=\begin{bmatrix}0&c\alpha&s\alpha&0&ls\beta s\alpha&-ls\beta c\alpha\end{bmatrix}\\ {}^1\mathbf{S}_{15}=\begin{bmatrix}1&0&0&0&lc\beta s\alpha&-lc\beta c\alpha\end{bmatrix}\\ {}^1\mathbf{S}_{16}=\begin{bmatrix}0&-s\alpha&c\alpha&lc\beta&ls\beta c\alpha&ls\beta s\alpha\end{bmatrix}\end{array}\right\} \tag{1}$$

where the first two twists are generated from the rT joint, the third is generated from the prismatic joint, and the last three are generated from the spherical joint. β is the angle between the limb (${}^1\mathbf{S}_{13}$) and its projection on plane ${}^1y{}^1o{}^1z$ passing through rT joint center and perpendicular to the bracket axis (${}^1x$), α is the angle between axis ${}^1y$ and the limb projection on plane ${}^1y{}^1o{}^1z$. l is the distance between the rT joint center and the spherical joint center. Labels $c\alpha$ and $s\alpha$ denote cosine(α) and sin(α), respectively. In the twist notation ${}^1\mathbf{S}_{ij}$, the first subscript i denotes the limb number, the second subscript j denotes the joint number within the limb and the leading superscript indicates the local frame.

The six screws in (1) form a six-system [36] and there is no reciprocal screw, showing that the $(rT)_1PS$ limb has six degrees of freedom (DOFs) and does not supply constraint to the platform connected to it.

For the $(rT)_2PS$ limb as in Fig. 1(b), the radial axis of the rT joint is collinear with the prismatic joint passing through the spherical joint center. Thus, the spherical joint center A cannot move out of the plane ${}^1y{}^1o{}^1z$. Based on the coordinate system in Fig. 1(b), the twist system of the $(rT)_2PS$ limb can be given as

$$\left\{{}^1\mathbf{S}_1\right\}=\left\{\begin{array}{l}{}^1\mathbf{S}_{11}=\begin{bmatrix}1&0&0&0&0&0\end{bmatrix}\\ {}^1\mathbf{S}_{12}=\begin{bmatrix}0&-c\alpha&-s\alpha&0&0&0\end{bmatrix}\\ {}^1\mathbf{S}_{13}=\begin{bmatrix}0&0&0&0&c\alpha&s\alpha\end{bmatrix}\\ {}^1\mathbf{S}_{14}=\begin{bmatrix}0&c\alpha&s\alpha&0&0&0\end{bmatrix}\\ {}^1\mathbf{S}_{15}=\begin{bmatrix}1&0&0&0&ls\alpha&-lc\alpha\end{bmatrix}\\ {}^1\mathbf{S}_{16}=\begin{bmatrix}0&-s\alpha&c\alpha&l&0&0\end{bmatrix}\end{array}\right\} \tag{2}$$

It is clear that twists ${}^1\mathbf{S}_{12}$ and ${}^1\mathbf{S}_{14}$ are the same and the six twists form a five-system [36]. Thus, there is one reciprocal screw to (2) in the limb constraint system as

$$\left\{{}^1\mathbf{S}_1^r\right\}={}^1\mathbf{S}_1^r=\begin{bmatrix}1&0&0&0&ls\alpha&-lc\alpha\end{bmatrix} \tag{3}$$

This gives a constraint force acting along a line passing through the spherical joint center with a direction parallel to the bracket axis of the rT joint. Thus, the $(rT)_2PS$ limb has five DOFs, one less than the $(rT)_1PS$ phase.

When constructing parallel mechanisms with the rT*PS* limbs, the mechanisms will have ability of mobility change by altering the rT*PS* limbs into these two phases. In the following, the $(rT)_2PS$ limb phases will be used by connecting the rT joints to the base with perpendicular bracket axes and the spherical joints to the moving platform. Then altering the limbs into the $(rT)_1PS$ phase will generate new mechanism topologies with mobility change.

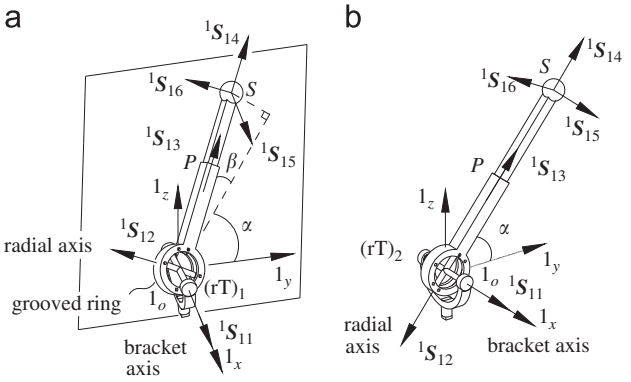

Fig. 1. Two phases of the rT*PS* limb. (a) $(rT)_1PS$ and (b) $(rT)_2PS$.

3. 3rT*PS* MPM with perpendicular constraint screws

3.1. Mobility analysis

The 3rT*PS* metamorphic parallel mechanism is shown in Fig. 2 with all limbs in phase $(rT)_2PS$. The three limbs are arranged symmetrically on three perpendicular planes with the bracket axes perpendicular to the planes as in Fig. 2.

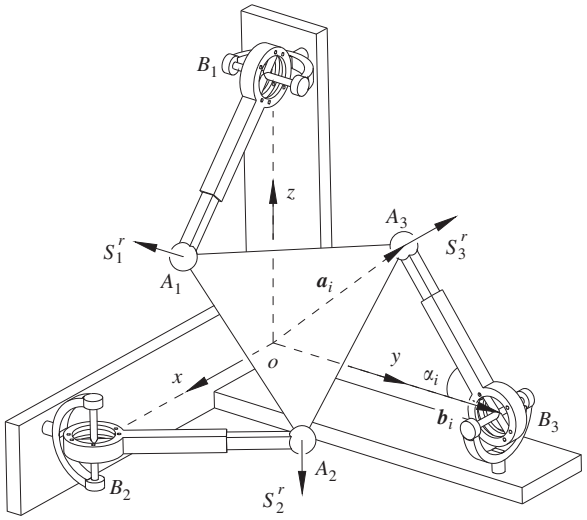

Fig. 2. The 3(rT)$_2$*PS* with three perpendicular constraint screws.

Let points A_i and B_i denote the spherical joint center and the rT joint center in limb i (i=1, 2, 3), respectively. Locate a global coordinate system *oxyz* at point *o* with *x*-axis passing through rT joint center B_2 in limb 2 and *y*-axis passing through rT joint center B_3 in limb 3 as in Fig. 2. Then, *z*-axis passes through rT joint center B_1 in limb 1. Let $\boldsymbol{a}_i$ and $\boldsymbol{b}_i$ denote the vectors of points A_i and B_i in the coordinate system *oxyz*, and l_i be the limb length between the spherical joint center A_i and the rT joint center B_i.

Based on the description in Fig. 2, the parameters expressed in the coordinate system *oxyz* can be given as

$$\begin{cases} \mathbf{b}_1=(0,0,r_b),\mathbf{a}_1=\mathbf{b}_1+l_1(\sin\alpha_1,0,-\cos\alpha_1) \\ \mathbf{b}_2=(r_b,0,0),\mathbf{a}_2=\mathbf{b}_2+l_2(-\cos\alpha_2,\sin\alpha_2,0) \\ \mathbf{b}_3=(0,r_b,0),\mathbf{a}_3=\mathbf{b}_3+l_3(0,-\cos\alpha_3,\sin\alpha_3) \end{cases} \tag{4}$$

where α_i is the angle between limb i and the line oB_i passing through the rT joint center B_i and the coordinate system origin *o*.

From (3), it can be seen that (rT)$_2$*PS* limb supplies one constraint force to the platform with the direction parallel to its bracket axis. Thus, the constraint system of the 3(rT)$_2$*PS* parallel mechanism in Fig. 2 can be given as

$$\mathbf{S}^r=\begin{Bmatrix} \mathbf{S}_1^r=\left[(0,1,0) \quad \mathbf{a}_1\times(0,1,0)\right] \\ \mathbf{S}_2^r=\left[(0,0,1) \quad \mathbf{a}_2\times(0,0,1)\right] \\ \mathbf{S}_3^r=\left[(1,0,0) \quad \mathbf{a}_3\times(1,0,0)\right] \end{Bmatrix}$$

$$=\begin{Bmatrix} \begin{bmatrix} 0 & 1 & 0 & l_1c\alpha_1-r_b & 0 & l_1s\alpha_1 \end{bmatrix}, \\ \begin{bmatrix} 0 & 0 & 1 & l_2s\alpha_2 & l_2c\alpha_2-r_b & 0 \end{bmatrix}, \\ \begin{bmatrix} 1 & 0 & 0 & 0 & l_3s\alpha_3 & l_3c\alpha_3-r_b \end{bmatrix} \end{Bmatrix} \tag{5}$$

which are three constraint forces perpendicular to each other.

By taking reciprocal screws to (5), motion screws of the mechanism can be obtained as

$$\mathbf{S}_m=\begin{Bmatrix} \begin{bmatrix} 1 & 0 & 0 & 0 & r_b-l_1c\alpha_1 & -l_2s\alpha_2 \end{bmatrix}, \\ \begin{bmatrix} 0 & 1 & 0 & -l_3s\alpha_3 & 0 & r_b-l_2c\alpha_2 \end{bmatrix}, \\ \begin{bmatrix} 0 & 0 & 1 & r_b-l_3c\alpha_3 & -l_1s\alpha_1 & 0 \end{bmatrix}. \end{Bmatrix} \tag{6}$$

which represent three rotational DOFs with directions parallel to the axes of the coordinate system *oxyz*.

Thus, the 3(rT)$_2$*PS* parallel mechanism with perpendicular constraint screws has mobility three with pure rotations, which is similar to the pyramid parallel mechanism [37] consisting of three *RPS* limbs in three perpendicular constraint planes.

3.2. Topology change of the 3rTPS MPM

Altering the (rT)$_2$*PS* limbs in the previous 3(rT)$_2$*PS* parallel mechanism into the phase (rT)$_1$*PS* will result in various new mechanism topologies with increased mobility. After changing the phase of limb 1, the 3(rT)$_2$*PS* parallel mechanism becomes the topology in Fig. 3 with name of 2(rT)$_2$*PS*–1(rT)$_1$*PS*.

Since the (rT)$_1$*PS* limb does not supply any constraint on the platform, the first constraint screw in (5) vanishes and the other two constraint forces in (5) are left on the platform as in Fig. 3. The reciprocity of this two-screw system gives one more motion screw than those three in (6) as

$$\mathbf{S}_{m1}=\begin{bmatrix} 0 & 0 & 0 & 0 & 1 & 0 \end{bmatrix} \tag{7}$$

which is a translation along *y*-axis.

Thus, the 2(rT)$_2$*PS*–1(rT)$_1$*PS* parallel mechanism has four DOFs with one translation and three rotations, which is one more DOF than the 3(rT)$_2$*PS* in Fig. 2. Hence, with the topology change from 3(rT)$_2$*PS* to 2(rT)$_2$*PS*–1(rT)$_1$*PS*, the mobility of the mechanism increases to one.

When further changing the phase of limb 2 to (rT)$_1$*PS*, the 2(rT)$_2$*PS*–1(rT)$_1$*PS* topology in Fig. 3 changes to the 1(rT)$_2$ *PS*–2(rT)$_1$*PS* in Fig. 4(a). Based on the platform constraint system in (5), only the third constraint screw is left and platform motion screw system has one more translation screw along *z*-axis than

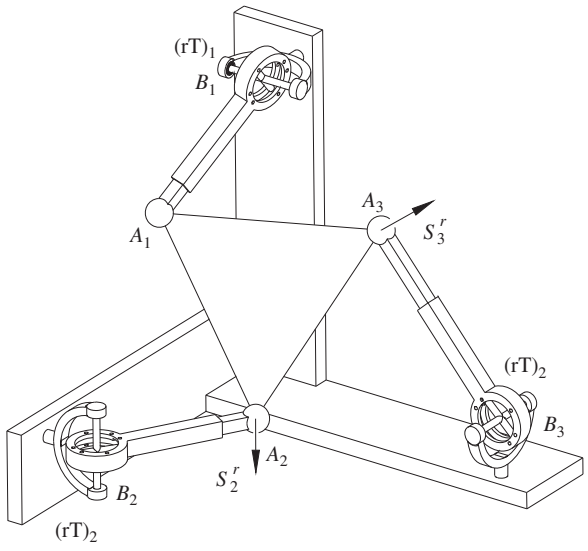

Fig. 3. The 2(rT)$_2$*PS*–1(rT)$_1$*PS* with two perpendicular constraint screws.

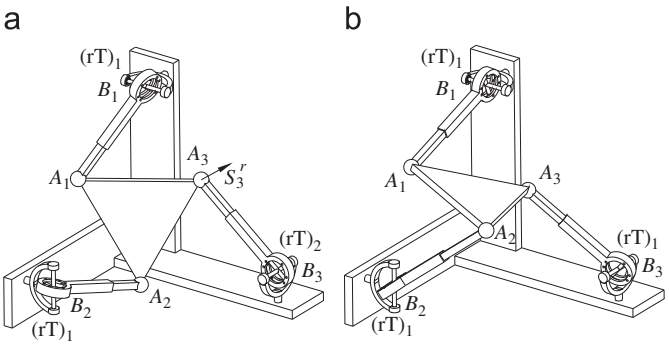

Fig. 4. Two more topologies of the 3r*TPS*. (a) 1(rT)$_2$*PS*–2(rT)$_1$*PS* and (b) 3(rT)$_1$*PS*.

those in (6) and (7). Thus, the $1(rT)_2PS$–$2(rT)_1PS$ parallel mechanism has five DOFs with two translations and three rotations, indicating that one more mobility gained after changing the topology from $2(rT)_2PS$–$1(rT)_1PS$ to $1(rT)_2PS$–$2(rT)_1PS$.

Finally, when changing the third limb to phase $(rT)_1PS$, the mechanism becomes another topology $3(rT)_1PS$ as in Fig. 4(b) with no constraint on the platform. Thus, the mechanism changes to the topology with mobility 6.

The foregoing analysis shows that when changing phases of limb 1, limb 2 and limb 3 one after another, the $3(rT)_2PS$ parallel mechanism changes to three other topologies with mobility change from 3 to 4, to 5 and then to 6. However, this only shows one procedure of topology change of the 3rT*PS* parallel mechanism. When changing the limb phases in different orders and with different numbers at the same time, the four topologies can be altered into any other. The rule is that there is the translation along y-axis when limb 1 is in phase $(rT)_1PS$ and it is constrained when limb 1 is in phase $(rT)_2PS$. Similarly, limb 2 and limb 3 correspond to the translation along z and x-axes, respectively. The combination of the phases of the three limbs contributes to different mechanism topologies with variable mobility.

Based on this, a mobility change map can be illustrated in Fig. 5, in which $3R1T_k$ means three rotations with one translation along k-axis, $3R2T_{ki}$ means three rotations with two translations along k and i-axes, and 3R3T represent full mobility 6. The double-arrow lines between any two mobility types indicate that any two of them can be changed into each other. For example, change from 3R to $3R2T_{xy}$ can be realized by altering phases of limb 1 and limb 3 from $(rT)_2PS$ to $(rT)_1PS$ at the same time based on the topology $3(rT)_2PS$ in Fig. 2. The obtained $1(rT)_2PS$–$2(rT)_1PS$ topology has three rotations and two translations along x and y-axes.

4. Actuation scheme for the reconfigurable topologies

Actuation inputs of a parallel mechanism work with limb constraints to determine the platform position and orientation. In the $(rT)_2PS$ limb, the rotation about the bracket axis or the translation along the prismatic joint can be used as inputs. Based on Fig. 1(b) and the limb motion screws in (2), these two inputs can result in constraint screws as

$$\begin{cases} {}^1\mathbf{S}^r_{rTba} = [0 \quad -s\alpha \quad c\alpha \quad l \quad 0 \quad 0] \\ {}^1\mathbf{S}^r_{Pa} = [0 \quad c\alpha \quad s\alpha \quad 0 \quad 0 \quad 0] \end{cases} \tag{8}$$

where ${}^1\mathbf{S}^r_{rTba}$, a constraint force passing through the spherical joint center and perpendicular to both the bracket axis and the limb, is the input constraint from the bracket axis rotation. ${}^1\mathbf{S}^r_{Pa}$, a constraint force along the limb, is the input constraint from the prismatic joint.

When altering the $(rT)_2PS$ limb to phase $(rT)_1PS$, one more actuation choice appears as the rotation about the radial axis with an input constraint force passing through the spherical joint center and parallel to the bracket axis as described by (3).

The rule for a satisfied actuation scheme is that the input constraint screws form a six-system with the platform constraint screw system. Based on this and the above analysis, the actuation scheme of the 3rT*PS* metamorphic parallel mechanism can be concluded: (a) $3+n$ actuation inputs are needed for the topology $(3\text{-}n)(rT)_2PS$–$n(rT)_1PS$; (b) any one of the three inputs (rotation about the bracket axis and translation of limb $(rT)_2PS$, rotation about the radial axis of limb $(rT)_1PS$) can be used as actuation; and (c) at least one of them should be from each $(rT)_1PS$ limb if there is.

To demonstrate the rule, the $1(rT)_2PS$–$2(rT)_1PS$ parallel mechanism in Fig. 4(a) can be taken as an example. Based on the scheme concluded, $3+2=5$ actuation inputs are needed for this topology, which can be chosen from the eight choices (the $(rT)_2PS$ limb has two, each $(rT)_1PS$ limb has three) and two of them should be from the two $(rT)_1PS$ limbs. Taking the three translations of the prismatic joints in the three limbs and the rotations about the radial axes of the two $(rT)_1PS$ limbs as an example, the actuation input constraint screw system can be given as

$$\mathbf{S}^r_a = \begin{Bmatrix} \mathbf{S}^r_{1Pa} = [\mathbf{u}_1 \quad \mathbf{b}_1 \times \mathbf{u}_1] \\ \mathbf{S}^r_{2Pa} = [\mathbf{u}_2 \quad \mathbf{b}_2 \times \mathbf{u}_2] \\ \mathbf{S}^r_{1rTra} = [\mathbf{u}_{b1} \quad \mathbf{a}_1 \times \mathbf{u}_{b1}] \\ \mathbf{S}^r_{2rTra} = [\mathbf{u}_{b2} \quad \mathbf{a}_2 \times \mathbf{u}_{b2}] \\ \mathbf{S}^r_{3Pa} = [\mathbf{u}_3 \quad \mathbf{b}_3 \times \mathbf{u}_3] \end{Bmatrix} \tag{9}$$

where $\boldsymbol{u}_i$ is the unit vector along limb i and can be expressed in (11), α and β are shown in Fig. 1. $\boldsymbol{u}_{bi}$ is the unit vector perpendicular to both limb i and its radial axis.

The five input force screws with the third geometric constraint screw in (5) form a six-system, showing that the selected actuation inputs can fix the required position and orientation of the platform. This also shows the validity for the unified kinematics modeling by choosing the rotation about the radial axis as input in the following section.

5. Unified kinematics modeling and displacement analysis

5.1. Unified kinematics modeling

Considering the difference between the two phases of the rT*PS* limb, it can be found that the key part is the rotation about the radial axis which can be represented by angle β as in Fig. 6. A limb coordinate system ${}^1o{}^1x{}^1y{}^1z$ is located at the rT joint center with ${}^1x$

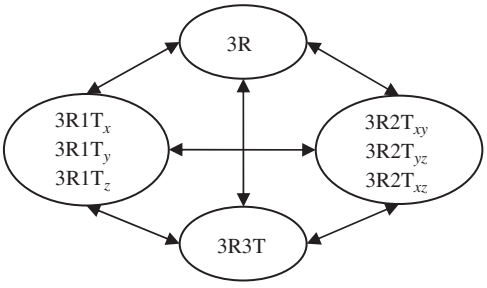

Fig. 5. Mobility change map.

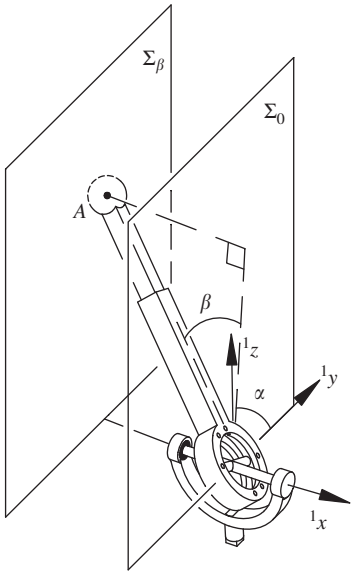

Fig. 6. Unified limb modeling.

axis collinear with the bracket axis and ^1y axis perpendicular to the bracket surface as in Fig. 6.

It can be taken as that the $(rT)_1PS$ limb has variable angle β while the $(rT)_2PS$ limb has a fixed angle $\beta=0$. Geometrically, spherical joint center A is constrained on plane $\sum\beta$ passing through the spherical joint center and perpendicular to the bracket axis for a giving angle β in the $(rT)_1PS$ limb and it is constrained on plane $\sum 0$ passing through the rT joint center and perpendicular to the bracket axis in the $(rT)_2PS$ limb. Based on Fig. 6, the spherical joint center A in the limb coordinate system $^1o^1x^1y^1z$ can be given as

$$^1\mathbf{a}=l(-\sin\beta,\cos\beta\cos\alpha,\cos\beta\sin\alpha)\begin{cases}\beta & (rT)_1PS\\ \beta=0 & (rT)_2PS\end{cases} \tag{10}$$

Based on the actuation analysis in Section 4, the rotation about the radial axis of the $(rT)_1PS$ limb can be used as actuation input. Thus, the $(rT)_2PS$ limb can be taken as a special configuration of the $(rT)_1PS$ limb by locking the actuation at $\beta=0$. This gives an important method to unify the geometric and kinematics modeling of the 3rT*PS* metamorphic parallel mechanism by covering all its reconfigurable topologies with mobility change. The following is to use the prismatic joint in the $(rT)_2PS$ limb as actuation input and the rotation about the radial axis is added for the second actuation when the limb changes to phase $(rT)_1PS$.

Based on the above analysis and the coordinate systems of the 3rT*PS* metamorphic parallel mechanism in Fig. 7, the geometric constraint of the mechanism can be given as

$$\begin{cases}\mathbf{a}_1=\mathbf{b}_1+R(z,-\pi/2)R(x,-\pi/2)l_1(-\sin\beta_1,\cos\beta_1\cos\alpha_1,\cos\beta_1\sin\alpha_1)\\ \mathbf{a}_2=\mathbf{b}_2+R(x,-\pi/2)R(z,\pi/2)l_2(-\sin\beta_2,\cos\beta_2\cos\alpha_2,\cos\beta_2\sin\alpha_2)\\ \mathbf{a}_3=\mathbf{b}_3+R(z,\pi)l_3(-\sin\beta_3,\cos\beta_3\cos\alpha_3,\cos\beta_3\sin\alpha_3)\end{cases}$$

$$\begin{cases}\beta_i & (rT)_1PS\\ \beta_i=0 & (rT)_2PS\end{cases} \tag{11}$$

where l_i is the limb length, $\mathbf{R}(k, g)$ represents a rotation about axis k with angle g and is used to translate the vector of the spherical joint center in the limb coordinate systems to the global coordinate system in Fig. 7.

5.2. Inverse and forward kinematics analysis

5.2.1. Inverse kinematics analysis

The inverse displacement analysis of the 3rT*PS* metamorphic parallel mechanism is to obtain the actuation parameters (limb length l_i, radial-axis rotation angle β_i) based on the given platform position and orientation. Attach a local coordinate system $o'x'y'z'$ at the centroid of the platform with x'-axis passing through spherical joint center A_1 and axis y' parallel to line A_2A_3 as in Fig. 8.

When giving the platform position $\boldsymbol{p}$ (p_x, p_y, p_z) and orientation $\mathbf{R}$ described in the global coordinate system in Fig. 7, the position of the spherical joint centers can be obtained as

$$\begin{cases}\mathbf{a}_1=\mathbf{p}+R.(r_a,0,0)\\ \mathbf{a}_2=\mathbf{p}+R.(-r_a/2,\sqrt{3}r_a/2,0)\\ \mathbf{a}_3=\mathbf{p}+R.(-r_a/2,-\sqrt{3}r_a/2,0)\end{cases} \tag{12}$$

where the spherical joint centers on the platform are symmetrically arranged on a circle with radius r_a.

It should be mentioned that, the platform position should be given based on the mechanism topology as analyzed in Section 3. The basic rule is that when limb 1 is in phase $(rT)_2PS$, position element p_y is constrained by the spherical joint center vector $\boldsymbol{a}_1$ with its element on y-axis $a_{1y}=0$. This is same for limb 2 with phase $(rT)_2PS$ and p_z is constrained by $a_{2z}=0$. In limb 3 with phase $(rT)_2PS$, p_x is constrained based on $a_{3x}=0$. The relation can be concluded as

$$\begin{cases}p_y=-r_{22}r_a & \text{limb 1 in } (rT)_2PS\\ p_z=r_{31}r_a/2-\sqrt{3}r_{32}r_a/2 & \text{limb 2 in } (rT)_2PS\\ p_x=r_{11}r_a/2+\sqrt{3}r_{12}r_a/2 & \text{limb 3 in } (rT)_2PS\end{cases} \tag{13}$$

where r_{ij} is the element with the ith row and jth column in the rotation matrix $\mathbf{R}$.

By correspondingly equaling (12) to (11), the inverse displacement analysis can be solved

$$\begin{cases}l_1=\sqrt{\mathbf{c}_1.\mathbf{c}_1},\\ l_2=\sqrt{\mathbf{c}_2.\mathbf{c}_2},\\ l_3=\sqrt{\mathbf{c}_3.\mathbf{c}_3},\end{cases}\quad\begin{cases}\beta_i=-\sin^{-1}(c_{ix}) & (rT)_1PS\\ \beta_i=0 & (rT)_2PS\end{cases} \tag{14}$$

$$\text{where}\begin{cases}\mathbf{c}_1=R(x,\pi/2)R(z,\pi/2)(\mathbf{a}_1-\mathbf{b}_1)\\ \mathbf{c}_2=R(z,-\pi/2)R(x,\pi/2)(\mathbf{a}_2-\mathbf{b}_2)\\ \mathbf{c}_3=R(z,-\pi)(\mathbf{a}_3-\mathbf{b}_3)\end{cases}$$

c_{ix} is the element of vector $\boldsymbol{c}_i$ on the x-axis, $\boldsymbol{a}_i$ is expressed in (12) and $\boldsymbol{b}_i$ is from (4).

5.2.2. Forward kinematics

On the contrary to the inverse displacement analysis, the forward one is to solve the platform position $\boldsymbol{p}$ (p_x, p_y, p_z) and orientation $\mathbf{R}$ when giving the corresponding actuation parameters (l_i, β_i) for each topology. Based on this and Fig. 8, the geometric constraint of the platform triangle can be described as

$$\begin{cases}d_{12}^2=(\mathbf{a}_1-\mathbf{a}_2)^2\\ d_{13}^2=(\mathbf{a}_1-\mathbf{a}_3)^2\\ d_{23}^2=(\mathbf{a}_2-\mathbf{a}_3)^2\end{cases}\quad\begin{cases}\beta_i & (rT)_1PS\\ \beta_i=0 & (rT)_2PS\end{cases} \tag{15}$$

Substituting (11) into (15) and replacing $\cos\alpha_i=(1-t_i^2)/(1+t_i^2)$,

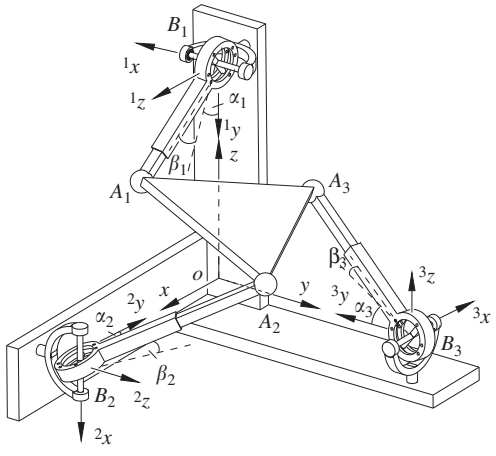

Fig. 7. Unified kinematics modeling of the 3rT*PS* with perpendicular constraint screws.

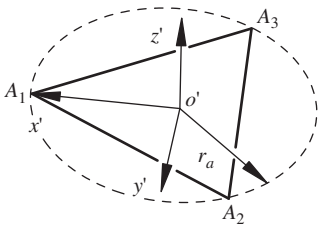

Fig. 8. The platform coordinate system.

Table 1
Inverse kinematics examples.

Topology	DOFs	Input parameters	Output parameters
$3(rT)_2PS$	3R	$\mathbf{R}_0$, ($\boldsymbol{p}_0$= (1.8171, 2.5022, 3.0925))	l_1=5, l_2=7, l_3=6
$2(rT)_2PS$–$1(rT)_1PS$	3R1T$_y$	$\mathbf{R}_0$, p_y= p_{0y}+1.4	l_1=5.19, l_2=7.55, l_3=4.99, β_1=0.273
$1(rT)_2PS$–$2(rT)_1PS$	3R2T$_{yz}$	$\mathbf{R}_0$, p_y= p_{0y}+1.4, p_z= p_{0z}+1.2	l_1=4.1865, l_2=7.642, l_3=5.963, β_1=0.341, β_2=0.1577
$3(rT)_1PS$	3R3T	$\mathbf{R}_0$, p_x= p_{0x}−1.3, p_y= p_{0y}+1.4, p_z= p_{0z}+1.2	l_1=3.7037, l_2=8.7987, l_3=6.103, β_1=0.3876, β_2=0.1368, β_3=−0.2146

$\sin\alpha_i=2t_i/(1+t_i^2)$, there is

$$\begin{cases} f_1(1,t_1,t_1^2,t_2^2,t_1t_2^2,t_1^2t_2^2)=0 \\ f_2(1,t_3,t_3^2,t_1^2,t_3t_1^2,t_3^2t_1^2)=0 \\ f_3(1,t_2,t_2^2,t_3^2,t_2t_3^2,t_2^2t_3^2)=0 \end{cases} \tag{16}$$

where $f_i(\bullet)$ is a linear function of the power product in the bracket with coefficients depending on known parameters only, t_i is $\tan(\alpha_i/2)$.

By using Sylvester's dialytic elimination method [38,39] for the first two equations in (16), there is

$$f_4(1,t_3,t_2^2,t_3^2,t_2^2t_3,t_3^3,t_2^4,t_3^4,t_2^2t_3^2,t_2^2t_3^3,t_2^4t_3^1,t_2^2t_3^4,t_2^4t_3^2,t_2^4t_3^3,t_2^4t_3^4)=0 \tag{17}$$

where $f_4(\bullet)$ is a linear function of the power product in the bracket with coefficients depending on known parameters only.

Then, following the same method for (17) and the third equation in (16), a polynomial with only unknown t_3 can be obtained as

$$\sum_{i=0}^{+16} h_i t_3^i = 0 \tag{18}$$

where coefficient h_i are real constants depending on input data only.

This shows that a univariate equation in t_3 of degree 16 is obtained.

Solving (18), 16 solutions for t_3 can be obtained. Then, t_2 can be solved by substituting each solution of t_3 back to the third equation in (16) and selecting the roots satisfying (17). Following this, t_1 can be solved by substituting each pair of solutions of t_2 and t_3 into the first equation in (16) with proof of the second equation in (16). Based on this, sixteen pair of solutions of t_1, t_2, t_3 are obtained and the spherical joint center A_i can be calculated by substituting α_i=2arctan(t_i) into (11). Then, the platform position and orientation can be determined using the three spherical joint centers with Fig. 8 as

$$\begin{cases} \mathbf{z}'=(\mathbf{a}_2-\mathbf{a}_1)\times(\mathbf{a}_3-\mathbf{a}_1)/\left|\left|(\mathbf{a}_2-\mathbf{a}_1)\times(\mathbf{a}_3-\mathbf{a}_1)\right|\right| \\ \mathbf{y}'=(\mathbf{a}_2-\mathbf{a}_3)/\left(\sqrt{3}r_a\right) \\ \mathbf{x}'=\mathbf{y}'\times\mathbf{z}' \\ R=(\mathbf{x}',\mathbf{y}',\mathbf{z}') \\ \mathbf{p}=\mathbf{a}_1-r_a\mathbf{x}' \end{cases} \tag{19}$$

The real roots correspond to assembly configurations of the 3rT*PS* parallel mechanism.

5.3. Numerical examples of the kinematics analysis

5.3.1. Inverse kinematics examples

Based on the kinematics analysis in Section 5.2, inverse kinematics examples for the four topologies of the 3rT*PS* metamorphic parallel mechanism can be given as in Table 1 to demonstrate the unified kinematics modeling. The structure parameters are set as: r_a=10, r_b=$2\sqrt{3}$. In the examples in Table 1, the four topologies correspond to the four in Figs. 2–4, which means that the $2(rT)_2PS$–$1(rT)_1PS$ is obtained by altering the phase of limb 1 from the topology $3(rT)_2PS$. Then, the $1(rT)_2PS$–$2(rT)_1PS$ is obtained by further altering the phase of limb 2. By giving the orientation and position parameters of the platform and using (14), the inverse kinematics can be solved with results in Table 1. The input rotation matrix is given as

$$R_0=\begin{bmatrix} 0.0861 & 0.5560 & 0.8267 \\ -0.7223 & -0.5366 & 0.4361 \\ 0.6862 & -0.6347 & 0.3554 \end{bmatrix} \tag{20}$$

which is used for all the topologies in Table 1.

From Table 1, $\boldsymbol{p}_0$ is the parasitic position of the $3(rT)_2PS$ parallel mechanism when giving the orientation $\mathbf{R}_0$. It can be seen that the number of input parameters increases with the mobility increasing in the topology change. Following this, the number of output parameters also increases with specific rotation angles (β_i) about the radial axes of the $(rT)_1PS$ limbs instead of value zero in the $(rT)_2PS$ phase.

Table 2
Forward kinematics solutions of $3(rT)_2PS$.

No.	t_1	t_2	t_3
1	−0.0242+0.6799*I	0.3989+0.4957*I	−1.951–0.7218*I
2	−0.0242–0.6799*I	0.3989–0.4957*I	−1.951+0.7218*I
3	0.1929–0.4598*I	0.5653–0.1*I	−0.1976–0.3454*I
4	0.1929+0.4598*I	0.5653+0.1*I	−0.1976+0.3454*I
5	0.3443–0.6502*I	−2.3758–0.1344*I	0.0042–0.6527*I
6	0.3443+0.6502*I	−2.3758+0.1344*I	0.0042+0.6527*I
7	−0.0046	−0.0784	0.046
8	0.4123 - 0.0323*I	−0.0416–0.1805*I	0.2592–0.2166*I
9	0.4123+0.0323*I	−0.0416+0.1805*I	0.2592+0.2166*I
10	0.2343–0.9106*I	0.3278–0.8633*I	0.29–0.8831*I
11	0.2343+0.9106*I	0.3278+0.8633*I	0.29+0.8831*I
12	−1.6752+0.8184*I	−0.0408–0.5657*I	0.3571–0.5329*I
13	−1.6752 - 0.8184*I	−0.0408+0.5657*I	0.3571+0.5329*I
14	0.2219	0.1569	0.358
15	−0.0911–0.3644*I	0.262–0.2656*I	0.5832–0.0657*I
16	−0.0911+0.3644*I	0.262+0.2656*I	0.5832+0.0657*I

5.3.2. Forward kinematics examples

In order to check the validity of the forward kinematics analysis, the same structure parameters and the output parameters in Table 1 in the inverse kinematics examples are used as the input for the forward kinematics examples. Following the procedures in Section 5.2.2, the forward kinematics can be solved. As for each topology, there are 16 solutions for the forward kinematics analysis, only the solutions for topology $3(rT)_2PS$ are listed in Table 2 as an example. Real solutions of all the topologies are listed in Table 3 with corresponding mechanism assemblies demonstrated in Fig. 9.

In Table 3, it can be found that one of the real solutions of the forward kinematics corresponds to the input one of the inverse kinematics examples in Table 1, indicating the closure validity of the inverse and forward kinematics analysis. This can be also seen in Fig. 9 that the orientation of the platform (green triangle) is the same in Fig. 9 (b), (d), (h) and (l), corresponding to the rotation matrix $\mathbf{R}_0$ in (20) which is the input of the inverse kinematics analysis in Table 1. In Fig. 9, the blue line is the base and the black lines represent the limbs, the platform coordinate system is showed

Table 3
Real solutions of forward kinematics.

Topology	Real solutions
$3(rT)_2PS$	$R_{11}=\begin{bmatrix}-0.3058 & 0.5142 & 0.8013\\ -0.2824 & -0.8527 & 0.4395\\ 0.9092 & -0.0918 & 0.4059\end{bmatrix}$; $\boldsymbol{R}_{12}=\boldsymbol{R}_0$; $\boldsymbol{p}_{11}$=(1.0131, 0.9782, 1.8505); $\boldsymbol{p}_{12}$= (1.8171, 2.5022, 3.0925).
$2(rT)_2PS–1(rT)_1PS$	$R_{21}=\begin{bmatrix}-0.2888 & 0.4111 & 0.8646\\ -0.1683 & -0.9108 & 0.3768\\ 0.9424 & -0.0366 & 0.3323\end{bmatrix}$; $\boldsymbol{R}_{22}=\boldsymbol{R}_0$; $\boldsymbol{p}_{21}$= (0.733, 1.983, 1.7424); $\boldsymbol{p}_{22}$= (1.8171, 3.9022, 3.0925).
$1(rT)_2PS–2(rT)_1PS$	$R_{31}=\begin{bmatrix}-0.1775 & 0.4282 & 0.8861\\ 0.0039 & -0.9001 & 0.4357\\ 0.9841 & 0.0808 & 0.1581\end{bmatrix}$; $R_{32}=\begin{bmatrix}0.1570 & 0.4216 & 0.8931\\ -0.0437 & -0.9004 & 0.4327\\ 0.9866 & -0.1070 & -0.1229\end{bmatrix}$; $R_{33}=\begin{bmatrix}0.2859 & 0.4304 & 0.8562\\ -0.4272 & -0.7425 & 0.5158\\ 0.8578 & -0.5132 & -0.0284\end{bmatrix}$; $\boldsymbol{R}_{34}=\boldsymbol{R}_0$; $\boldsymbol{p}_{31}$= (0.977, 1.386, 2.662); $\boldsymbol{p}_{32}$= (1.5367, 1.5516, 3.23); $\boldsymbol{p}_{33}$= (1.7862, 2.8797, 4.2254); $\boldsymbol{p}_{34}$= (1.8171, 3.9022, 4.292).
$3(rT)_1PS$	$R_{41}=\begin{bmatrix}0.1286 & 0.4409 & 0.8882\\ -0.0452 & -0.8921 & 0.4495\\ 0.9906 & -0.0979 & -0.0948\end{bmatrix}$; $R_{42}=\begin{bmatrix}0.2193 & 0.4371 & 0.8723\\ -0.0816 & -0.8827 & 0.4628\\ 0.9722 & -0.1727 & -0.1579\end{bmatrix}$; $R_{43}=\begin{bmatrix}0.3199 & 0.4307 & 0.8439\\ -0.1962 & -0.8413 & 0.5037\\ 0.9269 & -0.3267 & -0.1846\end{bmatrix}$; $\boldsymbol{R}_{44}=\boldsymbol{R}_0$; $\boldsymbol{p}_{41}$= (0.2457, 1.556, 3.2098); $\boldsymbol{p}_{42}$= (0.391, 1.683, 3.402); $\boldsymbol{p}_{43}$= (0.546, 2.079, 3.786); $\boldsymbol{p}_{44}$= (0.5171, 3.9022, 4.292).

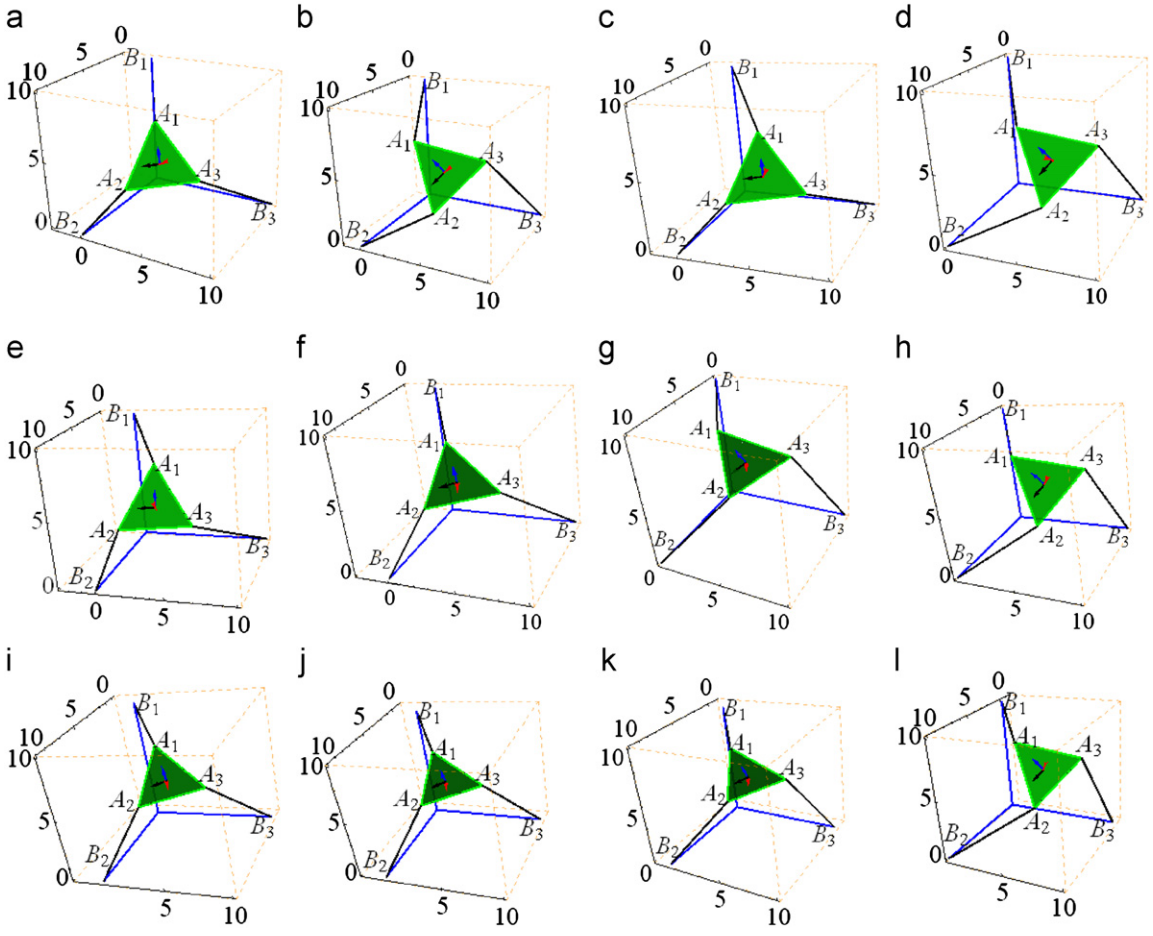

Fig. 9. Mechanism assemblies corresponding to the real solutions in Table 3. (a) ($\mathbf{R}_{11}$, p_{11}), (b) ($\mathbf{R}_{12}$, p_{12}), (c) ($\mathbf{R}_{21}$, p_{21}), (d) ($\mathbf{R}_{22}$, p_{22}), (e) ($\mathbf{R}_{31}$, p_{31}), (f) ($\mathbf{R}_{32}$, p_{32}), (f) ($\mathbf{R}_{33}$, p_{33}), (g) ($\mathbf{R}_{33}$, p_{33}), (h) ($\mathbf{R}_{34}$, p_{34}), (i) ($\mathbf{R}_{41}$, p_{41}), (j) ($\mathbf{R}_{42}$, p_{42}), (k) ($\mathbf{R}_{43}$, p_{43}) and (l) ($\mathbf{R}_{44}$, p_{44}). (For interpretation of the references to color in this figure caption, the reader is referred to the web version of this article.)

with blue arrow in x direction, black arrow in y direction and the red arrow in the z direction perpendicular to the platform plane.

6. Conclusions

This paper introduced a new metamorphic parallel mechanism named 3rT*PS* consisting of three reconfigurable rT*PS* limbs in perpendicular base planes. The rT*PS* limb had two working phases resulted from the configuration change of the reconfigurable Hooke (rT) joint. Screw theory was used to analyze mobility of the rT*PS* limb in its two phases, which showed that in one phase the rT*PS* limb has mobility 6 and in the other it had one DOF less, providing a constraint force to the platform. Based on this, the platform constraint screw system demonstrated the topology

change of the 3rT*PS* metamorphic parallel mechanism by altering the phases of the rT*PS* limbs, which illustrated that the mechanism had four topologies with ability of mobility change among 3R (three rotations), 3R1T (three rotations one translation), 3R2T and mobility 6. Following this, the actuation constraint screws showed that the rotations about the bracket axis and the radial axis, the translation of the prismatic joint can be chosen as the actuation input for the variety topologies. This gave the possibility of a unified kinematics modeling of the rT*PS* limb by choosing the rotation about the radial axis as the actuation and taking one phase as a special case of the other. Based on this, a unified kinematics modeling of the 3rT*PS* metamorphic parallel mechanism was obtained to cover all its four topologies. Analytical solutions of inverse and forward kinematics analysis were obtained. Numerical examples were used to demonstrate the analysis with mechanism configurations illustrated corresponding to the real solutions, which proved the validity of these theoretical results.

References

[1] Gough VE. Automobile stability, control, and tyre performance. Proceedings of Automobile Division, Institution of Mechanical Engineers 1956;171:392–4.
[2] Stewart D. A platform with six degrees of freedom. Journal of System Engineering and Control, Proceedings of the Institution of Mechanical Engineers 1965;180(15):371–86.
[3] Pierrot F, Fournier A, Dauchez P. Toward a fully parallel 6-DOF robot for high-speed applications. International Journal of Robotics & Automation 1992;7(1): 15–22.
[4] Huang T, Wang JS, Whitehouse DJ. Closed form solution to the workspace of hexapod-based virtual axis machine tools. ASME Journal of Mechanical Design 1999;121(1):26–31.
[5] Huang T, Li M, Zhao XM, Mei JP, Chetwynd DG, Hu SJ. Conceptual design and dimensional synthesis of 3-DOF module of the TriVariant—a novel 5-DOF reconfigurable hybrid robot. IEEE Transactions on Robotics 2005;21(3): 449–56.
[6] Dai JS, Kerr DR. Six-component contact force measurement device based on the Stewart platform. Proceedings of the Institution of Mechanical Engineers Part C: Journal of Mechanical Engineering Science 2000;214(5):687–97.
[7] Saglia JA, Dai JS, Caldwell DG. Geometry and kinematic analysis of a redundantly actuated parallel mechanism that eliminates singularities and improves dexterity. ASME Journal of Mechanical Design 2008;130 12450-1-5.
[8] Brandt G, Zimolong A, Carrat L, Merloz P, Staudte HW, Lavallee S, et al. CRIGOS: a compact robot for image – guided orthopedic surgery. IEEE Transactions on Information Technology in Biomedicine 1999;3(4):252–60.
[9] Merlet JP. Parallel robots. 2nd ed.Springer; 2008.
[10] Hunt KH. Structural kinematics of in-parallel-actuated robot-arms. ASME Journal of Mechanisms Transmissions and Automation in Design 1983;105: 705–12.
[11] Gan DM, Liao QZ, Dai JS, Wei SM. Design and kinematics analysis of a new 3CCC parallel mechanism. Robotica 2010;28(7):1065–72.
[12] Tsai LW. Solving the inverse dynamics of a Stewart-Gough manipulator by the principle of virtual work. ASME Journal of Mechanical Design 2000;122(1):3–9.
[13] Gosselin C. Determination of the workspace of 6-dof Parallel Manipulators. ASME Journal of Mechanical Design 1990;112:331–6.
[14] Liu XJ, Jin ZL, Gao F. Optimum design of 3-DOF spherical parallel manipulators with respect to the conditioning and stiffness indices. Mechanism and Machine Theory 2000;35(9):1257–67.
[15] Huang Z, Li QC. General methodology for the type synthesis of lower-mobility symmetrical parallel manipulators and several novel manipulators. International Journal of Robotics Research 2002;21(2):131–45.
[16] Kong X, Gosselin CM. Type synthesis of 3-DOF spherical parallel manipulators based on screw theory. ASME Journal of Mechanical Design 2004;126(1):101–8.
[17] Chen IM, Li SH, Cathala A. Mechatronic design and locomotion of Amoebot—a metamorphic underwater vehicle. Journal of Robotic Systems 2003;20(6): 307–14.
[18] Gan DM, Dai JS, Liao QZ. Mobility analysis of two types of metamorphic parallel mechanisms. ASME Journal of Mechanisms and Robotics 2009;1 041007_1-9.
[19] Wohlhart K. Kinematotropic linkages. In: Lenarcic J, Parenti-Castelli V, editors. Advances in Robot Kinematics. Dordrecht: Kluwer; 1996. p. 359–68.
[20] J.S. Dai, J.J. Rees, Mobility in metamorphic mechanisms of foldable/erectable kinds, In: Proceedings of 25th ASME biennial mechanisms and robotics conference, Atlanta, GA, September 1998. (also in ASME Journal of Mechanical Design, 121(3) (1999) 375–382.).
[21] J.J. Parise, L.L. Howell, S.P. Magleby, Ortho-planar mechanisms, In: Proceedings of 26th biennial mechanisms and robotics conference, Baltimore, MD, September, Paper No. DETC2000/MECH-14193.
[22] C. Liu, T. Yang, Essence and characteristics of metamorphic mechanisms and their metamorphic ways, In: Proceedings of 11the World Congress in Mechanism and Machine Science, Tianjing, China, April, 2004, pp. 1285–1288.
[23] Dai JS, Rees JJ. Matrix representation of topological changes in metamorphic mechanisms. ASME Journal of Mechanical Design 2005;127(4):837–40.
[24] Yan HS, Kuo CH. Topological representations and characteristics of variable kinematic joints. ASME Journal of Mechanical Design 2006;128(2):384–91.
[25] Kuo CH, Yan HS. On the mobility and configuration singularity of mechanisms with variable topologies. ASME Journal of Mechanical Design 2007;129:617–24.
[26] Fanghella P, Galletti C, Giannotti E. Parallel robots that change their group of motion. In: Lenarčič J, Parenti-Castelli V, editors. Advances in Robot Kinematics: Mechanisms and Motion. Dordrecht: Springer; 2006. p. 49–56.
[27] Refaat S, Hervé JM, Nahavandi S, Trinh H. Two-mode over-constrained three-Dofs rotational-translational linear-motor-based parallel-kinematics mechanism for machine tool applications. Robotica 2007;25(4):461–6.
[28] Kong XW, Gosselin CM, Richard PL. Type synthesis of parallel mechanisms with multiple operation modes. ASME Journal of Mechanical Design 2007; 129(6):595–601.
[29] Dai JS, Wang D. Geometric analysis and synthesis of the metamorphic robotic hand. ASME Journal of Mechanical Design 2007;129(11):1191–7.
[30] Zhang LP, Wang DL, Dai JS. Biological modeling and evolution based synthesis of metamorphic mechanisms. ASME Journal of Mechanical Design 2008;130:1–11 072303.
[31] Zhang KT, Dai JS, Fang YF. Topology and constraint analysis of phase change in the metamorphic chain and its evolved mechanism. ASME Journal of Mechanical Design 2010;132(12):1–11 121001.
[32] D.M. Gan, J.S. Dai, China Patent, 2011, Application Number 201110054834.7.
[33] Gan DM, Dai JS, Liao QZ. Constraint analysis on mobility change of a novel metamorphic parallel mechanism. Mechanism and Machine Theory 2010; 45(12):1864–76.
[34] Gan DM, Dai JS, Caldwell DG. Constraint-based limb synthesis and mobility-change aimed mechanism construction. ASME Journal of Mechanical Design 2011;133(5) 051001_1-9.
[35] Dai JS, Huang Z, Lipkin Harvey. Mobility of overconstrained parallel mechanisms. ASME Journal of Mechanical Design 2006;128:220–9.
[36] Dai JS, Rees JJ. Interrelationship between screw systems and corresponding reciprocal systems and applications. Mechanism and Machine Theory 2001;36:633–51.
[37] Huang Z, Fang YF. Kinematic characteristics analysis of 3-DOF in-parallel actuated pyramid mechanisms. Mechanism and Machine Theory 1996;31(8): 1009–18.
[38] Bottema O, Roth B. Theoretical kinematics. New York: North-Holland; 1979.
[39] Gan DM, Liao QZ, Dai JS, Wei SM, Seneviratne LD. Forward displacement analysis of the general 6-6 Stewart mechanism using Grobner bases. Mechanism and machine theory 2009;44(9):1640–7.